Magnetotransport spectroscopy of spatially coincident coupled electron waveguides

S. F. Fischer,* G. Apetrii, and U. Kunze
Werkstoffe und Nanoelektronik, Ruhr-Universität Bochum, D-44780 Bochum

D. Schuh and G. Abstreiter
Walter Schottky Institut, Technische Universität München, Am Coulombwall, D-85748 Garching
(Received 8 December 2004; published 27 May 2005)

Magnetotransport spectroscopy is carried out on quantum point contacts fabricated from a 30-nm-wide square quantum well with two occupied two-dimensional subbands. In this system the spatial region of one-dimensional mode coupling is well defined and the two-dimensional reservoirs do not cause interferences. The magnetodispersions in transversal and longitudinal magnetic fields show crossings and anticrossings of the energy levels of the two one-dimensional subladders depending on the parity of the lateral modes of the wave functions. The influence of the quantum point contact geometry and persistent charging effects on coupling is demonstrated.

DOI: 10.1103/PhysRevB.71.195330 PACS number(s): 73.63.Nm, 72.20.My, 73.21.Hb, 73.23.Ad

I. INTRODUCTION

Coupling of one-dimensional (1D) electron systems in electron waveguides leads to wave-function mixing and splitting of degenerate energy levels. Two generic cases have to be considered: first, spatially separated tunnel-coupled, and, second, spatially coincident 1D electron systems. Coupling phenomena of electron waveguides are of fundamental interest in exploring two-level systems[1] under electric and magnetic fields as well as in future applications in quantum information processing.[2–4] Advances in nanolithography led to well-defined and controllable ballistic 1D electron systems such as quantum point contacts (QPCs) with high 1D subband separations,[5] a prerequisite to experimentally resolve coupling-induced energy splittings. Below, we report on magnetotransport spectroscopy of unprecedented resolution, allowing the proper identification of heretofore unresolved subtle interference induced by coupling of spatially coincident 1D electron systems.

To date, mainly tunnel-coupled *spatially separated* 1D electron systems have been investigated.[6–10] Vertically stacked and coupled QPCs were prepared from two-dimensional electron gas (2DEG) bilayer systems built from two GaAs quantum wells (QWs) separated by AlGaAs (Refs. 6–9) or AlAs (Ref. 9) barriers, or from a wide GaAs QW giving rise to a "soft" barrier via Coulomb repulsion.[10] Therein, mode coupling is induced by wave-function overlap determined by the height and width of the tunnel barrier and can emerge for degenerate energy levels of the 1D subladders. 1D energy level crossing or anticrossing is discussed in terms of symmetry considerations.[7] Despite such advances the separate and sole control of 1D mode coupling poses a predominant challenge for the fabrication of quantum devices based on mode-coupling phenomena. In vertically stacked electron systems mode coupling can occur in the 1D channel as well as in the 2D reservoirs because the tunnel barrier exists in both regions. Instead, laterally tunnel-coupled electron waveguides could immediately pave the way. However, to date, an experimental realization of precise mode coupling in laterally tunnel-coupled electron waveguides remains to be demonstrated.

Here, we explore unsettled coupling phenomena of *spatially coincident* 1D electron systems. In such systems mode coupling in the 2D reservoirs cannot occur in the absence of a magnetic field. The preparation and control of coherent quantum states exclusively develops in the 1D channel. Therefore, these systems inherently fulfil a major demand for quantum information processing. QPCs are prepared from a two-dimensional electron gas with occupied ground and first excited subbands. Hence, two subladders of discrete 1D energy levels evolve in the 1D constriction, which we specify in the following as the two *vertical* modes indexed by the quantum number *s*, as depicted in the schematic view of Figs. 1(a) and 1(b).

For coincidence of 1D energy levels, indexed by the quantum number *n*, originating from different vertical modes *s*, crossings or anticrossings are expected depending on the symmetry of the 1D confining potential. For harmonic potentials wave functions are separable and no mode coupling is expected, as previously investigated[11] by a QPC prepared from a single 2DEG with two occupied 2D subbands in a parabolic QW. For nonharmonic potentials, instead, complicated spectra of wave-function mixing in magnetic fields are predicted[12] and were demonstrated by spectroscopy experiments[13] on zero-dimensional electron systems. We study the complex hybrid case of coupling of spatially coincident electron waveguides for which the 1D confining potential is approximately harmonic in the lateral direction but asymmetric in the vertical (heterostructure growth) direction. As shown below, nearly regular patterns of crossings and anticrossings exist, depending on the parity of the lateral wave-function modes in the regime investigated.

II. EXPERIMENTAL DETAILS

QPCs are fabricated from a 30-nm-wide square QW with two 2D subbands populated with electrons. A conventional $GaAs/Al_{0.32}Ga_{0.68}As$ heterostructure (Si δ doped) contains the GaAs QW 60 nm below the sample surface. The as-grown carrier mobility in the dark at 4.2 K is 8.5

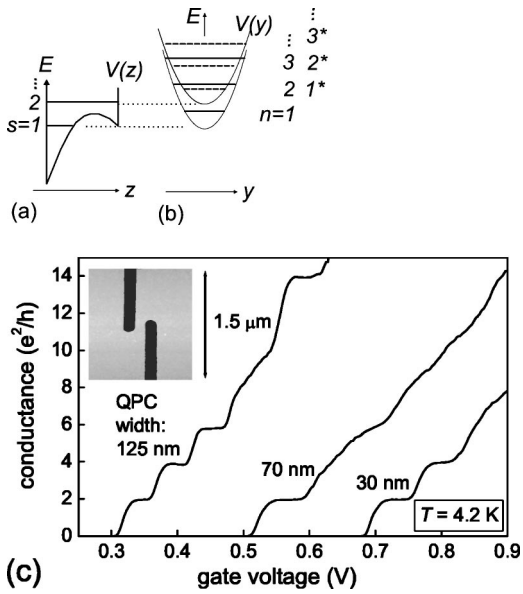

FIG. 1. Schematically (a) conduction band edge of the quantum well hosting a 2DEG with occupied ground and first excited subbands leading to (b) two subladders of 1D energy levels in a 1D constriction. (c) Quantized conductance corrected by series resistances of 500–600 Ω of three QPCs of different widths at 4.2 K. The inset shows an AFM image of the groove pattern defining the QPC.

$\times 10^5$ cm^2/V s at a density of 4.2×10^{11} cm^{-2}. The simulated band structure forms a symmetric QW in the conduction band edge at a small positive top-gate voltage V_g of about 0.1 V. For smaller and larger V_g the QW changes into an asymmetric, i.e., triangular, shape. The QW carrier density as a function of increasing V_g was formerly determined from Shubnikov–de Haas oscillations,[14] proving the filling of the ground subband at −0.4 V and at about +0.02 V of the first excited subband.

Narrow 1D constrictions are defined by dynamic ploughing with an atomic force microscope (AFM) and subsequent wet-chemical etching.[15] QPCs of geometric widths between 30 and 230 nm at an etch depth of 70–85 nm lead to 1D electron systems with large subband spacings in excess of 10 meV.[5] Consequently, well-defined quantized conductance steps and large conductance plateaus at multiples of $2e^2/h$ at 4.2 K prove high-quality ballistic transport for all of the fabricated QPCs. Such 1D electron systems are designated to resolve clearly splitting energies due to coupling.

The two-terminal differential drain conductance $g_d = \partial I_d/\partial V_d$ (at constant gate voltage V_g), where I_d and V_d denote source-drain current and voltage, respectively, and the transconductance $g_m = \partial I_d/\partial V_g \propto \partial g_d/\partial V_g$ (at constant V_d) have been measured as a function of V_g by means of a standard lock-in technique. The rms drain excitation voltage was 0.3 mV at 433 Hz. For transconductance measurements the gate voltage has additionally been modulated with a 3 mV rms ac voltage.

III. RESULTS

A remarkable feature of the conductance of QPCs prepared from a 2DEG with two occupied subbands are deviations from the regular increase in $2e^2/h$ units, such as missing or ill-defined steps, which arise from degeneracies of 1D energy levels of the two ladders or from their close proximity. Figure 1(c) shows the conductance characteristics of three QPCs containing the contributions of the two 1D ladders. Each 1D subladder has its own threshold voltage and subsequent 1D level population increases the conductance in $2e^2/h$ steps. Hence, from high-precision transconductance measurements we identify unambiguously the QPC modes by evaluating the transconductance maxima in terms of peak heights, half-widths, and positions.[14]

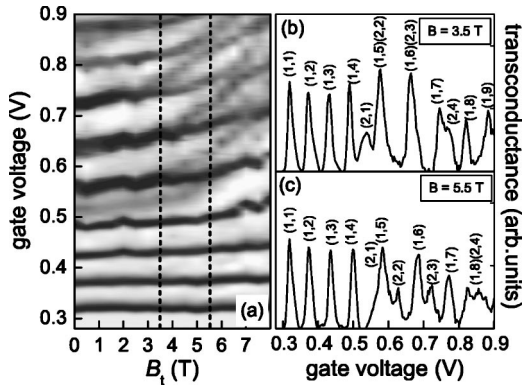

FIG. 2. (a) Transconductance gray-scale plot of a 125-nm-wide QPC vs applied *transversal* magnetic field and gate voltage at 2 K. The white regions represent low transconductance (conductance plateaus) and the dark traces represent high transconductance (transitions between conductance plateaus). (b) and (c) transconductance traces along the two dashed lines in (a) at two constant transverse magnetic fields of (b) $B_t = 3.5$ T and (c) $B_t = 5.5$ T. The index (s,n) associates each tranconductance maximum with a 1D subband. s describes the quantization in the growth direction (vertical modes) and n describes the lateral confinement (transverse modes). Note the clear (1,7)(2,3) and (1,8)(2,4) anticrossings in the gray-scale plot.

Most information about waveguide coupling can be extracted from magnetotransport spectroscopy by directly imaging the magnetodispersion, as shown in Fig. 2(a), Fig. 5(a) and Fig. 6. Here, the advantage of high 1D-subband spacing becomes immediately evident as level anticrossings are clearly visible and can be quantified. Consequently, we present magnetotransport in constant transversal magnetic field B_t, i.e., in the plane of the QW and perpendicular to the current flow in the 1D constriction, and in constant longitudinal magnetic field B_l, i.e., parallel to the 1D current flow.

First, magnetotransport in a *transversal* magnetic field B_t establishes insight into the 1D-level degeneracy and wavefunction mixing.

Figure 2(a) shows a transconductance gray-scale plot as a function of V_g and B_t for a 125 nm QPC. In Figs. 2(b) and 2(c) we show two transconductance vs gate voltage scans for $B_t = 3.5$ and 5.5 T, respectively. Bright areas in the gray-scale plot represent low transconductance values, i.e., conductance plateau regions. Dark lines, instead, depict transconductance maxima, corresponding to transitions between conductance plateaus which are associated with the successive 1D-subband edges passing through the Fermi level with increasing V_g. Distinct magnetodispersions related to the two independent 1D-subband ladders are evident from Fig. 2(a): the

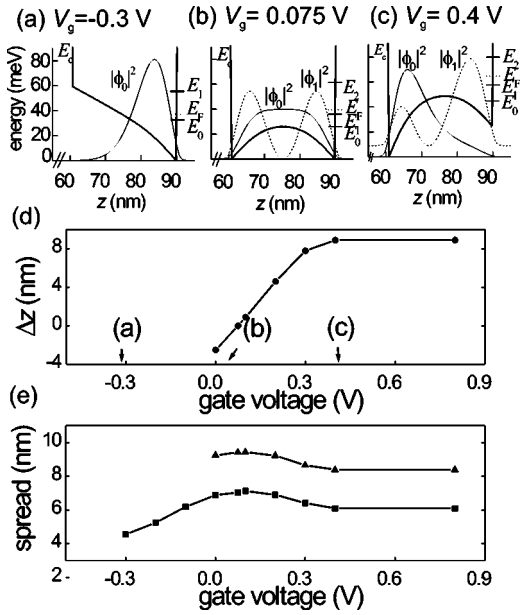

FIG. 3. Characteristic properties of the 30-nm-wide GaAs quantum well varying with applied top gate voltage at $T=2$ K. (a)–(c) Conduction band edge E_c, Fermi level E_F, subband energies E_0, E_1, and E_2, and square amplitudes of the electron wave functions ϕ_0 and ϕ_1 in the lowest and first excited 2D subbands. (d) The resulting difference Δz of the expectation values of electron distance for the ground and first excited 2D subbands and (e) the spread of the wave functions for the ground subband (square symbols) and the first excited subband (triangular symbols).

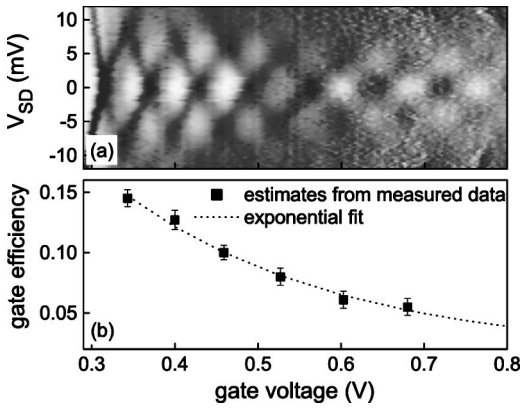

FIG. 4. (a) Transconductance gray-scale plot of the 125-nm-wide QPC vs gate voltage and applied dc source-drain voltage. The white regions correspond to low transconductance and the dark regions correspond to high transconductance. (b) Gate efficiency γ_1 for the first 1D ladder. The dotted line represents an exponential fit of the estimated data.

transconductance maxima corresponding to the second subband ladder shift more strongly to higher V_g with increasing B_t. This observation finds a straightforward explanation in terms of the diamagnetic energy shift, which is proportional to B_t^2 and to the square spread of the wave function in the growth direction.[16] In analogy to the larger spatial extent of the second 2D-subband wave function in the growth direction due to the formation of a triangular well at positive V_g, we anticipate a larger diamagnetic shift for the 1D levels of the second vertical mode. Figures 3(a), 3(b), and 3(c) show the calculated variation of the conduction band edge of the QW with applied top-gate voltage.[17]

Figure 3(d) depicts the difference in the expectation value of the electron distance from the upper heterointerface of the first excited and the ground 2D subbands $\Delta z=\langle z_1\rangle-\langle z_0\rangle$, where $\langle z_q\rangle=\int z\phi_q^2(z)dz/\int\phi_q^2(z)dz$ and ϕ_q denotes the wave function of the qth subband. Due to the asymmetric well potential this distance is larger for the first excited subband than for the ground state for gate voltages larger than 0.075 V. The spatial extent (spread) of the wave functions $(\langle z_q^2\rangle-\langle z_q\rangle^2)^{1/2}$ is shown in Fig. 3(e) for both subbands $q=0$, 1. Clearly, the wave-function spread of the first excited 2D subband exceeds that of the ground state. In order to discuss the consequences of the asymmetry in the quantum well potential for the magnetodispersion of 1D constrictions, we assign in the following the indices (s,n) to the vertical (s) and the transverse (n) quantization as depicted in Figs. 2(b) and 2(c). Note, in the 1D constriction $q=0$ corresponds to $s=1$, the first vertical mode, and $q=1$ to $s=2$, the second vertical mode. Due to the enhanced diamagnetic shift of the second vertical mode degeneracies of 1D energy levels of the two subband ladders are induced or abandoned with varying B_t. We observe level crossing for modes of unequal parity of the lateral modes, as given in Fig. 2(a) for modes (1,5)(2,2) or (1,6)(2,3) [see also Fig. 2(b) at $V_g=0.58$ and 0.66 V]. Anticrossings, instead, occur for lateral modes of equal parity, such as in Fig. 2(a) for, first, (1,8)(2,4) [see also Fig. 2(c) at $V_g=0.84$ V], second, (1,7)(2,3) (for $V_g=0.78$ V and $B_t=6.5$ T), and third, (1,6)(2,2). However, for (1,5)(2,1) the situation is somewhat ambiguous as neither level crossing nor anticrossing is clearly distinguishable. Generally, for most samples level coincidences of the first vertical mode with the lowest level of the second vertical mode (2,1) either render indistinguishable or tend to reveal crossings.

The anticrossings denoted by (1,7)(2,3) and (1,8)(2,4) in Fig. 2 are quantified by a doubled transconductance peak of reduced amplitude on the gate voltage scale by ΔV_g of 33 and 30 mV, respectively. In order to associate an energy splitting ΔE to the observed level anticrossings we transform the gate voltage scale into energy units. A variation of the gate voltage dV_g brings about a variation $dE_F=\gamma e(dV_g)$ of the Fermi energy, where γ denotes the gate efficiency and e the elementary charge. We determine the gate efficiency for the first 1D-subband ladder using gray-scale plots of the transconductance versus V_g and an applied dc source-drain voltage V_d [Fig. 4(a)].

The conductance was measured as a function of V_g at constant V_d and the transconductance was obtained by numerical differentiation. In Fig. 4(a) 1D energy separations are displayed by V_d values for which the conductance plateaus at multiples of $2e^2/h$ disappear and half plateaus at even multiples of e^2/h remain.[18,19] Furthermore, Fig. 4(a) is a direct superposition image generated by two 1D electron systems. In order to extract the gate efficiency γ_1 for the first vertical mode, we determine $\Delta E_{n,n+1}^1$, and the corresponding gate voltage interval ΔV_g at which the Fermi level sweeps $\Delta E_{n,n+1}^1$ from the transconductance versus V_g plot for $V_d=0$ V. Therefore, γ_1 results for $V_g=(V_{g,n}+V_{g,n+1})/2$ as the

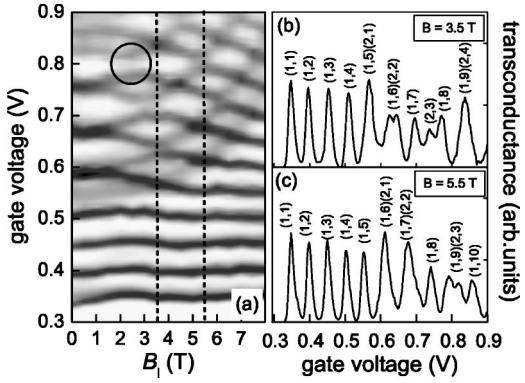

FIG. 5. (a) Transconductance gray-scale plot of a 125-nm-wide QPC vs applied *longitudinal* magnetic field and gate voltage at 2 K. The white and dark regions represent low and high transconductance, respectively. (b) and (c) transconductance traces along the two dashed lines in Fig. 2(a) at (b) B_l=3.5 T and (c) B_l=5.5 T. The index (s,n) associates each tranconductance maximum with a 1D subband. s describes the vertical modes and n describes the transverse modes. Note that examples for the clear anticrossings are (1,6)(2,2) and (1,7)(2,3) for B_l=3.5 T and (1,9)(2,3) for B_l=5.5 T in the transconductance traces and in the gray-scale plot, where (1,8)(2,4) has been additionally encircled.

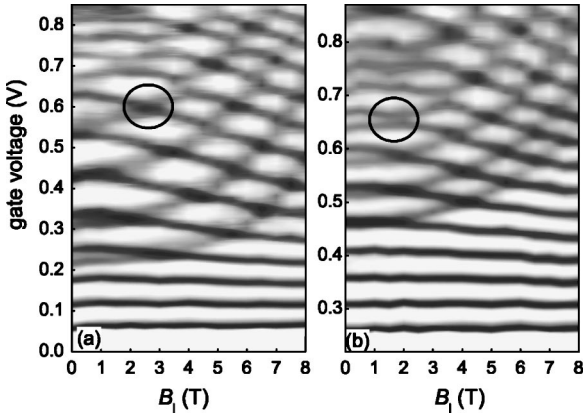

FIG. 6. Transconductance gray-scale plots of a 165-nm-wide QPC (groove etch depth 70 nm) vs applied *longitudinal* magnetic field and gate voltage at 2 K. A different confining potential of the same QPC is realized by persistent charging, i.e., cooling from RT to 2 K under applied gate bias (a) 0 and (b) +0.5 V. This causes a relative shift of the 1D subladders and enables us to observe the transformation from a crossing to an anticrossing situation of degenerate energy levels, as encircled in (a) and (b) for (1,8)(2,4).

ratio between $\Delta E^1_{n,n+1}$ and $e\Delta V_g$. Figure 4(b) shows the resulting values γ_1 and an exponential fit which concordantly describes the decrease of $\gamma_1(V_g)$ and allows an extrapolation to V_g values at which anticrossings occur. A determination of the gate efficiency for the second vertical mode $\gamma_2(V_g)$ is obscured by the fact that corresponding transconductance maxima appear much weaker in gray-scale presentation and render any evaluation unreliable. A similar gate efficiency for both 1D ladders would lead to an upper bound for the energy splitting ΔE of 1.2 meV (±0.3 meV). However, in Fig. 2(a) at B_t=0 T we observe larger spacings between consecutive maxima of the second ladder compared to that for the first ladder for $V_g \leqslant 0.7$ V. Given that the 1D energy separations of the two vertical modes are expected nearly equal to a first approximation a reduced gate efficiency is anticipated for the second vertical mode. From $g_m(V_g)$ at B_t=0 T we estimate a ratio γ_1/γ_2 of about 1.5 in the gate voltage region with the anticrossings. In consequence, we obtain a lower bound of 0.8 meV (±0.2 meV) for the energy splittings ΔE observed in transverse magnetic field.

Magnetotransport in a *longitudinal* magnetic field B_l is studied in analogy. However, the longitudinal magnetic field couples the lateral and vertical confinement of 1D electron motion, and distinctly different magnetodispersions are expected.[7,11] Figure 5(a) shows a transconductance gray-scale plot as a function of V_g and B_l for the 125 nm QPC discussed above. For increasing longitudinal magnetic field transconductance maxima corresponding to the first vertical mode shift to lower V_g, while those assigned to the second vertical mode shift to higher V_g. In Figs. 5(b) and 5(c) we present two of the measured transconductance vs gate voltage scans which show two clear anticrossings (1,6)(2,2) and (1,9)(2,3), respectively. In analogy to the evaluation of splitting energies in transverse magnetic fields we determine for the encircled anticrossing (1,8)(2,4) in Fig. 5(a) upper and lower bounds of 1.7 and 1.2 meV, respectively. In Fig. 5(a) level crossings and anticrossings show a regular pattern resembling the observations in transverse magnetic fields, i.e., anticrossing for lateral mode indices of equal parity. In other QPC samples regular patterns persist also for longitudinal magnetic fields; however, showing anticrossings for lateral modes of unequal parity (cf. Fig. 6).

This finding originates from the variation of the saddle-point potential of a 1D constriction as a consequence of the geometric variation of the etched nanoscale grooves or the variation of effective doping due to a persistent charging effect. In the following we briefly demonstrate examples for both cases.

Increasing the geometric width w of a QPC leads to a decrease in 1D-subband spacings which is correlated to a decrease in threshold voltage as was shown recently.[15] Note, w is only a good measure to compare QPCs with similar etch depths d of the nanoscale grooves. In spatially coincident electron waveguides a decrease in threshold voltage is observed for both vertical modes with increasing geometric QPC width w. However, in tendency this variation is less for the second vertical mode than for the first as visible from Fig. 7 (left ordinate).

Therefore the difference of threshold voltages between the first and second vertical mode is enhanced for increasing w [Fig. 7 (right ordinate)]. The difference in threshold voltages is determined, on one hand, by the 2D threshold in the reservoirs (as indicated in Fig. 7) and, on the other hand, by the nonidentical lateral confining potentials for the two vertical modes inside the 1D constriction. While the first depends on the effective doping level of the supply layer, the latter is a function of the geometry of the etched grooves as well as the ionized donor concentration.

An example of variations in the magnetodispersion due to a change in QPC geometry can be seen in Fig. 5(a) (w =125 nm, d=80 nm) and Fig. 6(a) (w=165 nm, d=70 nm).

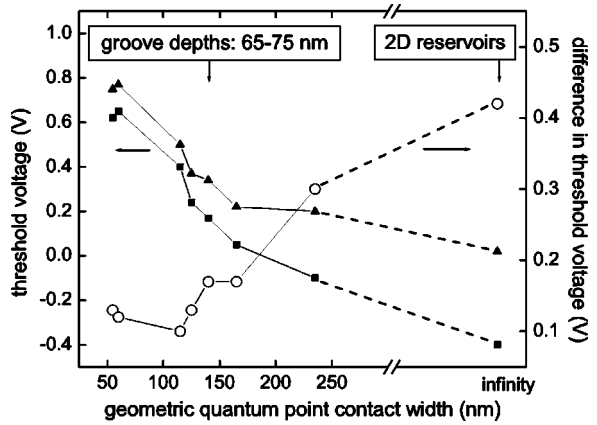

FIG. 7. A decrease of the threshold voltage with increasing geometric width of the QPC is observed for both vertical modes (left ordinate). However, the second vertical mode (filled triangles) shows less variation than the first (filled squares) which leads to an increase of the difference in threshold voltages with increasing geometric width of a QPC (right ordinate).

In Fig. 6(a) anticrossings occur for lateral modes of unequal parity. Note, the anticrossing (1,8)(2,4) of Fig. 5(a) has turned unambiguously into a crossing (encircled) in Fig. 6(a). Such deviations occur mainly in the regime of higher voltages in longitudinal magnetic fields.

By contrast, the confining potential of the same QPC can be tuned such that a relative shift of the 1D subladders of the two vertical modes occurs by purely electrostatic means.[14] Persistent charging can be achieved by cooling the sample from room temperature (RT) to low temperatures while applying a gate bias[20] and leads to a change in the effective doping. Figures 6(a) and 6(b) display the variation in the magnetodispersion of a QPC cooled without and with positive applied gate bias, respectively. The relative shift of 1D subladders leads to a larger difference of the threshold voltages for the first and second vertical modes. Furthermore, the change in confining potential can lead to a transition from a level crossing to anticrossing as observed for (1,8)(2,4) (encircled).

IV. DISCUSSION

Below, we discuss how the coupling phenomena under investigation are related to the observations from previous works on other 1D electron systems. A close resemblance is found for tunnel-coupled electron waveguides for which Thomas *et al.*[7] report coupling phenomena and splitting energies in transversal and longitudinal magnetic fields. Here, anticrossings in transversal magnetic fields are found only for 1D levels of *equal* lateral mode index. This is in accordance with a model of well-aligned saddle-point potentials of approximately equal confining strengths for which 1D levels of any combination of unequal lateral mode indices remain degenerate and show crossings. We do find such only-crossing cases for level degeneracies arising from the *first level* of the second vertical mode, $(1,n)(2,1)$. Therefore, we conclude that in these cases nearly similar 1D confining potentials exist, which is a rare situation that can only occur at lower or intermediate gate voltage as is outlined in the following. The ideal description of a 1D confining potential within the saddle-point potential approximation leads to equidistant 1D level spacings within one ladder. If the 1D confining potential is exactly the same for both vertical modes then additionally equal 1D separations exist for both 1D ladders. However, in our experiments two effects must cause corrections in most cases. First, as outlined in Fig. 3(d) the expectation value of the electron distance from the upper heterointerface is larger for the first excited 2D subband ($q=1$) than for the ground subband ($q=0$). Consequently, electrons in the 1D constriction experience a weakened lateral confinement for the second vertical mode ($s=2$) compared with the first ($s=1$), and hence, we expect slightly smaller 1D level separations for the second 1D ladder. Second, anharmonicity of the nonideal confining potential as well as its modification with increasing gate voltage[18,20] lead to a decrease in 1D energy spacings with increasing level index n within a 1D ladder. On behalf of these corrections the case of different lateral harmonic confining potentials for the two electron waveguides becomes relevant. For such, anticrossings are expected for 1D levels of equal parity in the lateral mode index (i.e., odd/odd or even/even). This corresponds to our observation of all anticrossings that occur under transversal magnetic fields in our experiments.

Apart from the common observations, tunnel-coupled 1D electron systems differ distinctly from electron waveguides with two vertical modes: first, a larger spatial separation of the expectation values of the electron position in the 1D constrictions exists and, second, nearly equal electron densities in the coupled waveguides can be adjusted. Until now, the sole previous work on spatially coincident electron waveguides was on QPCs prepared from a parabolic QW.[11] As in our study, in these systems the two vertical modes are populated by differing electron densities. However, due to the nearly parabolic QW no mode coupling is expected and within the regime of an undisturbed harmonic 1D confining potential all level degeneracies (crossings) persist.

It is worth mentioning that in all works cited above, a lateral 1D confinement was electrostatically defined by means of split, mid, or side gates prepared via electron-beam lithography and eventually supported by back gates. Gate widths exceeding 0.3 μm and deeply buried QWs result in rather weak 1D confining potentials and, hence, lead to 1D-subband spacings of only a few meV. Therefore energy splittings at anticrossings of 1D modes are difficult to resolve. Here, AFM nanolithography substantially improves the experimental resolution by providing high 1D-subband spacings in an extremely narrow lateral potential well.

V. CONCLUSION

In conclusion, we performed direct high-resolution imaging of distinct 1D energy level crossings and anticrossings of *spatially coincident* electron waveguides prepared from a nonharmonic, asymmetric 2D potential. By transport experiments, we have shown that the perturbation of symmetry via purely electrostatic means presents a powerful tool for a

high-precision adjustment of mode coupling between 1D quantum states. The two 1D electron systems experience strong coupling and strikingly nearly regular patterns of *mode-dependent* level anticrossings with distinct deviations are observed in transverse and longitudinal magnetic fields. While magnetotransport is a simple method to directly image a large energy interval in which two 1D subladders are shifted relative to each other, it is not the only one. The prospects of the spatially coincident electron waveguides will become immediately evident when mode coupling is turned on and off by purely electrostatic means. For this purpose structures with sophisticated combinations of gates (side, split, back gates) will be required.

ACKNOWLEDGMENTS

G.A. gratefully acknowledges the financial support of the Deutsche Forschungsgemeinschaft via Graduiertenkolleg 384. Part of this work was supported by the Bundesministerium für Bildung und Forschung under Grant No. 01BM920.

*Electronic address: Saskia.Fischer@rub.de

[1] E. Merzbacher, in *Quantum Mechanics*, 2nd ed. (Wiley, New York, 1970), pp. 428–429.
[2] J. Harris, R. Akis, and D. K. Ferry, Appl. Phys. Lett. **79**, 2214 (2001).
[3] A. Bertoni, P. Bordone, R. Brunetti, C. Jacoboni, and S. Reggiani, Phys. Rev. Lett. **84**, 5912 (2000).
[4] M. J. Gilbert, R. Akis, and D. K. Ferry, Appl. Phys. Lett. **81**, 4284 (2002).
[5] U. Kunze, Superlattices Microstruct. **31**, 3 (2002).
[6] I. M. Castleton, A. G. Davies, A. R. Hamilton, J. E. F. Frost, M. Y. Simmons, D. A. Ritchie, and M. Pepper, Physica B **249-245**, 157 (1998).
[7] K. J. Thomas, J. T. Nicholls, M. Y. Simmons, W. R. Tribe, A. G. Davies, and M. Pepper, Phys. Rev. B **59**, 12 252 (1999).
[8] M. A. Blount, J. S. Moon, J. A. Simmons, S. K. Lyo, J. R. Wendt, and J. L. Reno, Physica E (Amsterdam) **6**, 689 (2000).
[9] K. J. Friedland, T. Saki, Y. Hirayama, and K. H. Ploog, Physica E (Amsterdam) **11**, 144 (2001).
[10] S. Roddaro, V. Piazza, F. Beltram, W. Wegscheider, C.-T. Liang, and M. Pepper, J. Appl. Phys. **92**, 5304 (2002).
[11] G. Salis, T. Heinzel, K. Ensslin, O. J. Herman, W. Bchtold, K. Maranowski, and A. C. Gossard, Phys. Rev. B **60**, 7756 (1999).
[12] M. Robnik, J. Phys. A **19**, 3619 (1986).
[13] W. Hansen, T. P. Smith III, K. Y. Lee, J. A. Brum, C. M. Knoedler, J. M. Hong, and D. P. Kern, Phys. Rev. Lett. **62**, 2168 (1989).
[14] G. Apetrii, S. F. Fischer, U. Kunze, D. Schuh, and G. Abstreiter, Physica E (Amsterdam) **22**, 398 (2004).
[15] G. Apetrii, S. F. Fischer, U. Kunze, D. Reuter, and A. D. Wieck, Semicond. Sci. Technol. **17**, 735 (2002).
[16] F. Stern and W. E. Howard, Phys. Rev. **163**, 816 (1967).
[17] The calculations were performed using a program for self-consistent simulation of semiconductor nanostructures; M. Rother, computer code AQUILA Walter Schottky Institute, Technical University of Munich, 1999, available at http://www.mathworks.com/matlabcentral/fileexchange/loadFile.do?objectId=3344&objectType=FILE.
[18] N. K. Patel, J. T. Nicholls, L. Martn-Moreno, M. Pepper, J. E. F. Frost, D. A. Ritchie, and G. A. C. Jones, Phys. Rev. B **44**, 13 549 (1991).
[19] K. J. Thomas, M. Y. Simmons, J. T. Nicholls, D. R. Mace, M. Pepper, and D. A. Ritchie, Appl. Phys. Lett. **67**, 109 (1995).
[20] S. F. Fischer, G. Apetrii, S. Skaberna, U. Kunze, D. Reuter, and A. D. Wieck, Appl. Phys. Lett. **81**, 2779 (2002).